CHEMISTRY OF MATERIALS

ARTICLE

pubs.acs.org/cm

Controlled Synthesis of the Tricontinuous Mesoporous Material IBN-9 and Its Carbon and Platinum Derivatives

Yunfeng Zhao,[†] Daliang Zhang,[‡] Lan Zhao,[§] Guangchao Wang,[§] Yihan Zhu,[†] Amy Cairns,[†] Junliang Sun,[⊥] Xiaodong Zou,[⊥] and Yu Han*[,†]

[†]Advanced Membrane and Porous Materials Center, King Abdullah University of Science and Technology, Thuwal 23955-6900, Saudi Arabia

[‡]State Key Laboratory of Inorganic Synthesis and Preparative Chemistry, College of Chemistry, Jilin University, Changchun 130012, People's Republic of China

[§]Core Lab of Imaging and Characterization, King Abdullah University of Science and Technology, Thuwal 23955-6900, Saudi Arabia

[⊥]Berzelii Centre EXSELENT on Porous Materials and Inorganic and Structural Chemistry Unit, Department of Materials and Environmental Chemistry, Stockholm University, SE-106 91 Stockholm, Sweden

Supporting Information

ABSTRACT: Controlled synthesis of mesoporous materials with ultracomplicated pore configurations is of great importance for both fundamental research of nanostructures and the development of novel applications. IBN-9, which is the only tricontinuous mesoporous silica with three sets of interpenetrating three-dimensional channel systems, appears to be an excellent model mesophase for such study. The extensive study of synthesis space diagrams proves mesophase transition among the cylindrical MCM-41, tricontinuous IBN-9 and bicontinuous MCM-48, and also allows a more precise control of phase-pure synthesis. On the other hand, rational design of structure-directing agents offers a possibility to extend the synthesis conditions of IBN-9, as well as tailor its pore size. Moreover, an unprecedented helical structure consisting of twisted 3-fold interwoven mesoporous channels is reported here for the first time. The unique tricontinuous mesostructure of IBN-9 has been well-replicated by other functional materials (e.g., carbon and platinum) via a "hard-templating" synthesis route. The obtained carbon material possesses large surface area (~1900 m^2/g), high pore volume (1.56 cm^3/g), and remarkable gas adsorption capability at both cryogenic temperatures and room temperature. The platinum material has an ordered mesostructure composed of highly oriented nanocrystals.

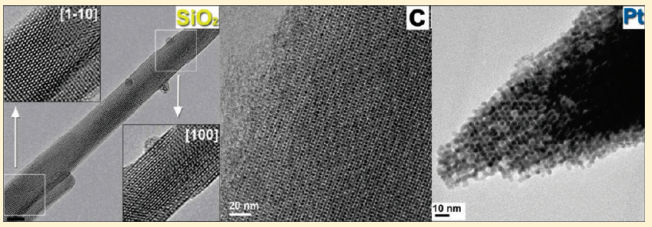

KEYWORDS: mesoporous materials, tricontinuous structure, hard template, surfactant

INTRODUCTION

Periodically ordered mesoporous silica materials are synthesized via the cooperative assembly of organic surfactants and inorganic silicate species, which allows the solidification of diverse flexible liquid crystal structures by hard materials.[1−8] A large variety of mesoporous structures have been fabricated by choosing different surfactant templates and varying the synthesis conditions. The most easily obtained as well as the simplest structure is two-dimensional (2-D) hexagonal (*p6mm*), consisting of hexagonally arranged one-dimensional (1-D) cylindrical mesoporous channels; the typical representatives are MCM-41 and SBA-15.[1,7] However, most mesoporous silicas have cage-type pores. The cages are interconnected by small windows to form three-dimensional (3-D), mostly cubic (e.g., $Fm\bar{3}m$,[9] $Im\bar{3}m$,[10] $Pm\bar{3}n$,[11] $Fd\bar{3}m$[12]) structures. Besides the 1-D channels and 3-D cages, another important family of mesoporous silica is "bi-continuous", which refers to the existence of two identical 3-D channels that are interwoven with each other but separated by a single continuous silica wall. The silica wall usually follows a three-periodic minimal surface. For example, MCM-48 has two interpenetrating chiral channels that are separated by a continuous silica wall following the gyroidal (G) minimal surface.[13,14] Thus, MCM-48 and the G-surface have the same topological structure and symmetry (cubic $Ia\bar{3}d$). Other mesoporous silicas defined by the G-surface include KIT-6[15] and FDU-5[16] that are prepared from triblock copolymer systems and have larger channel diameters than MCM-48. AMS-10 represents another type of "bi-continuous" structure; its silica wall follows the diamondoid (D) minimal surface (cubic $Pn\bar{3}m$).[17] Bicontinuous structure associated with the primitive (P) minimal surface

Received: June 12, 2011
Revised: June 29, 2011
Published: July 20, 2011

(cubic $Im\bar{3}m$) has also been found in a mesoporous aluminosilicate material.[18] These three "bi-continuous" mesoporous structures are all of cubic symmetry and their structural analogies have been extensively observed in surfactant-in-water systems.[19−23]

Ordered mesoporous structures consist of spatially well-defined arrays of both inorganic species (silicates in the wall) and organic molecules (surfactants in the cages/channels). The inorganic and organic arrays meet at an interface. The curvature of the interface would determine the type of mesostructure; for example, a continuous increase in surface mean curvatures could lead to lamellar—bicontinuous—cylindrical—globular (cagelike) mesophase transitions.[24,25] The interface curvature is governed by the interaction between surfactant molecules and silicate species.[26] Hence, the charge density and molecular geometry of surfactants are important structure-determining factors for the discovery of new mesoporous structures.[27] The first tricontinuous mesoporous silica IBN-9 with hexagonal $P6_3/mcm$ symmetry was synthesized by a specially designed surfactant template in our recent work.[28,29] It has the most complicated structure among all reported mesoporous materials, containing three identical interpenetrating 3-D channel systems. The three channels are separated by a single silica wall that follows a recently proposed "branched hexagonal (H) minimal surface".[30−33] Notably, such a 3-fold interpenetrating (tricontinuous) mesostructure has only been predicted mathematically but never been synthesized in real materials before, not even in soft matter such as surfactant-in-water system, block copolymers, or liquid crystals.

IBN-9 is the first—and currently only—tricontinuous mesoporous material. A thorough understanding of this material, in terms of structural features and synthetic conditions, would shed light on the fabrication of similar or more-complex multicontinuous mesostructures[31] and their applications. In the present work, we carefully investigated (i) the synthesis space diagrams with emphasis on the phase transitions between IBN-9 and its two neighboring mesophases, bicontinuous MCM-48, and cylindrical MCM-41; (ii) the extension of synthetic conditions and pore size adjustment by which a 3-D helical mesoporous structure has been fabricated for the first time; and (iii) the application of IBN-9 in nanocasting synthesis. A novel mesoporous carbon material with large BET surface area was successfully derived, which replicates the tricontinuous structure as well as the nanofiber morphology of IBN-9 but exhibits a "superstructure" that may be associated with the displacement of the tricontinuous carbon networks. Similar synthesis of mesostructured platinum was also studied.

EXPERIMENTAL SECTION

Syntheses of Surfactants. Four different surfactants have been synthesized (see Scheme 1), including (S)-(1-tetradecylcarbamoyl-2-phenyl-ethyl)-dimethyl-ethyl-ammonium bromide (denoted as S2-C14), and its two analogs S2-C16 and S2-C18 with longer hydrocarbon chains. The fourth surfactant is (S)-(1-tetradecylcarbamoyl-2-phenyl-ethyl)-triethyl-ammonium bromide (denoted as S3-C14), which has the same molecular structure as S2-C14, except for a slightly larger headgroup.

The detailed synthesis procedure for S2-C14 can be found in our previous work.[28] Surfactants S2-C16 and S2-C18 were synthesized using similar procedures, except that hexadecylamine and octadecylamine were used, respectively, instead of tetradecylamine. Surfactant S3-C14 was synthesized from Boc-L-phenylalanine in four steps and the details are given in the *Supporting Information*.

Scheme 1. Surfactants Used for the Synthesis of Mesoporous Silica

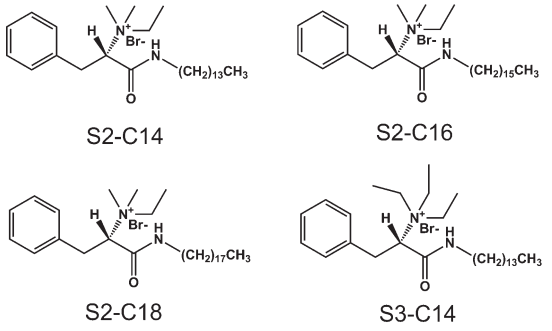

Syntheses of Mesoporous Silica Materials. A series of mesoporous silica materials have been synthesized in ammonia solution using the aforementioned surfactants as template and tetraethoxysilane (TEOS) as a silica source. Different mesostructures were fabricated by varying the type of surfactant, the amount of surfactant, the concentration of ammonia solution, and reaction temperature. In a typical synthesis of IBN-9, 40 mg of surfactant S2-C14 were dissolved in 12 mL of aqueous ammonia solution (2.0 wt %) at 45 °C. Next, 0.15 mL of TEOS was added dropwise under a static condition. The mixture was kept at 45 °C for 24 h under static conditions, and then aged at 100 °C in an autoclave for another 24 h. The obtained white flocculates were filtered, washed with water, dried in air, and calcined at 550 °C for 5 h to remove the surfactant. The effects of synthesis conditions on the mesostructures were carefully investigated and the results were summarized in the synthesis space diagrams (see the Results and Discussion section).

"Hard-Templating" Syntheses of Mesoporous Carbon and Pt. Mesostructured carbon and platinum materials (denoted as IBN-9-C and IBN-9-Pt, respectively) were synthesized using IBN-9 as a "hard template". The typical synthesis procedure of IBN-9-C is as follows. One milliliter (1 mL) of acetone solution containing 2 mg of 4-toluene sulfonic acid was impregnated into 200 mg of calcined IBN-9 silica powder. The mixture was dried at room temperature and then mixed with 1 mL of acetone containing 0.2 mL of furfural alcohol, followed by acetone evaporation at room temperature. The obtained powder was heated at 423 K for 2 h to polymerize furfural alcohol (4-toluene sulfonic acid was the catalyst for the polymerization), and then transferred into a tube furnace where it was carbonized with N_2 flow at 1173 K for 2 h. Finally, the silica template was removed by 10 wt % hydrofluoric acid (HF). The remaining carbon material was washed thoroughly with distilled water and dried in air. IBN-9-Pt was synthesized by following a reported method while using IBN-9 instead of MCM-48 as the template.[51]

Materials Characterization. Transmission electron microscopy (TEM) and selected-area electron diffraction (SAED) were performed on a FEI Titan electron microscope operated at 300 kV. The TEM specimens were prepared by dispersing the mesoporous silica powders in ethanol and dropping the resulting suspension onto a 200-mesh holey carbon-coated copper grid. Ultramicrotomy was conducted in a Leica EM UC6 system to cut IBN-9 nanofibers into slices, which allowed for TEM imaging along the fiber axis direction. Scanning electron microscopy

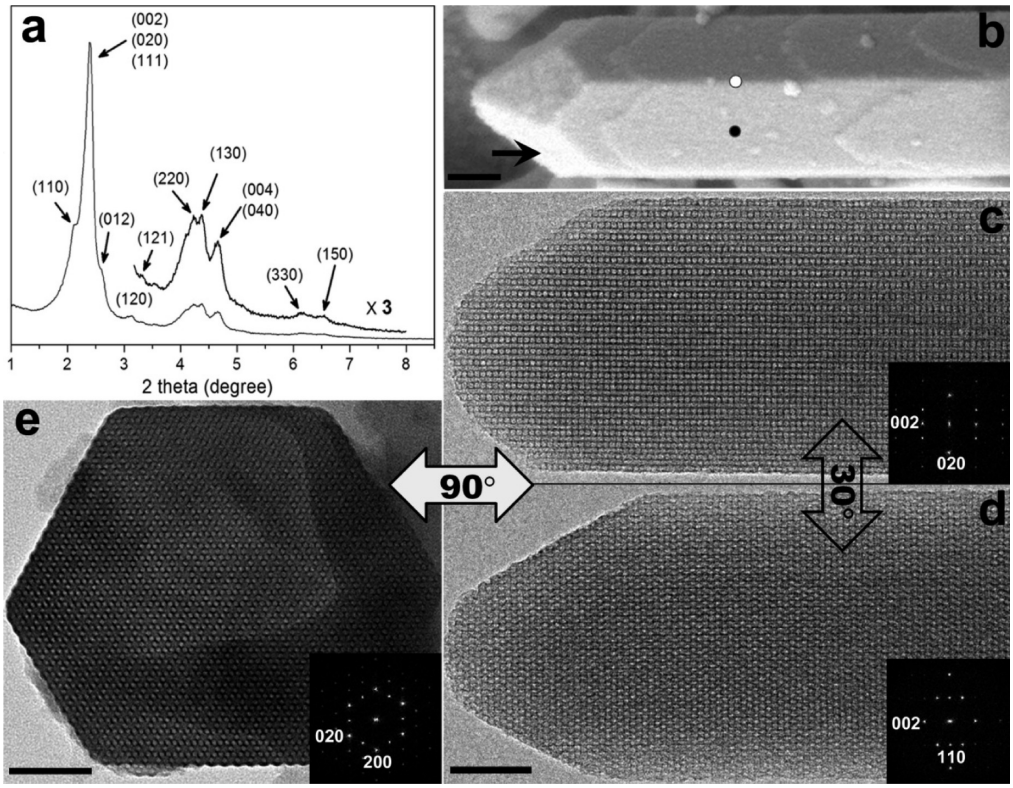

Figure 1. (a) Indexed powder XRD pattern of IBN-9. (b) SEM image taken at the end of an IBN-9 fiber. The marked white dot, black dot, and arrow indicate the respective directions along which the HRTEM images in panels (c), (d), and (e) were taken. (c−e) HRTEM images of IBN-9 taken along the (c) [100], (d) [1$\bar{1}$0], and (e) [001] directions. Inserts are the corresponding Fourier diffractograms. The angular relationships between the images are also indicated. The scale bars correspond to 50 nm.

(SEM) was conducted on a FEI Quanta 600 electron microscope operated at 30 kV. Powder X-ray diffraction (XRD) patterns were collected on a Bruker D8 Advance diffractometer equipped with a NaI dynamic scintillation detector using Cu Kα radiation. Nitrogen adsorption−desorption isotherms were obtained at liquid nitrogen temperature (77 K), using a Micromeritics ASAP 2020 M system. The pore size distribution came from the analysis of the adsorption branch of the isotherm. Argon sorption was conducted at 87 K on a fully automated micropore gas analyzer Autosorb-1 MP (Quantachrome Instruments). Low-pressure H_2 adsorption and CO_2 adsorption studies were performed on the same instrument. The complex mesoporous structures of MCM-48, IBN-9, and IBN-9-C were resolved by electron crystallography based on high-resolution TEM (HRTEM) images.[34] The detailed methods have been elaborated in our recent publication.[28b]

RESULTS AND DISCUSSION

Description of the Mesostructures. Four types of mesoporous silicas have been prepared using surfactant S2-C14 as a template under different synthetic conditions. One of them has a disordered structure, while the other three possess highly ordered, specifically, tricontinuous hexagonal, bicontinuous cubic, and cylindrical 2-D hexagonal structures, which were respectively named IBN-9, IBN-6, and IBN-10 in our previous work.[28] Since IBN-6 and IBN-10 are structural analogies of the well-known MCM-48 and MCM-41, we use, in this paper, the conventional terms (i.e., MCM-48 and MCM-41) to denote the two materials for general understandability.

IBN-9 was synthesized in ammonia solutions of low concentration (<10 wt %). When synthesized from the typical conditions, IBN-9 crystals exhibited fiber morphology with widths of 70−300 nm and lengths of 5−20 μm. The XRD pattern showed 10 discernible peaks, indicating a highly ordered mesostructure (Figure 1a).[28] The high-resolution SEM image taken at the end of a fiber clearly shows a pencil-tip-like shape with a 6-fold axis (Figure 1b). Three HRTEM images are shown in Figures 1c−e with their incidence directions and angular relationships marked in the SEM image (Figure 1b). The structure of IBN-9 has been successfully resolved by electron crystallography based on the HRTEM images.[28] The results reveal that IBN-9 is hexagonal ($P6_3/mcm$) with a = 88.4 Å and c = 84.3 Å, having a rather complicated structure consisting of three congruent mesoporous channel systems interwoven with each other (see Figures S1a−c in the Supporting Information).

MCM-48 could also be prepared from the typical synthesis conditions for IBN-9 by simply using a more concentrated ammonia solution (25 wt %), as determined by the XRD and HRTEM images (see Figure 2). The 3D electrostatic potential map reconstructed from the HRTEM images confirms the bicontinuous structure (see Figure S1d in the Supporting Information). Comparing the topological similarity and difference between MCM-48 and IBN-9 might be helpful for understanding the evolution from bicontinuous to tricontinuous structure, which is yet unclear. Figure 3 shows two fragments isolated from the **etc-c3** net of IBN-9 and the **srs-c** net

dx.doi.org/10.1021/cm2016593 |*Chem. Mater.* 2011, 23, 3775–3786

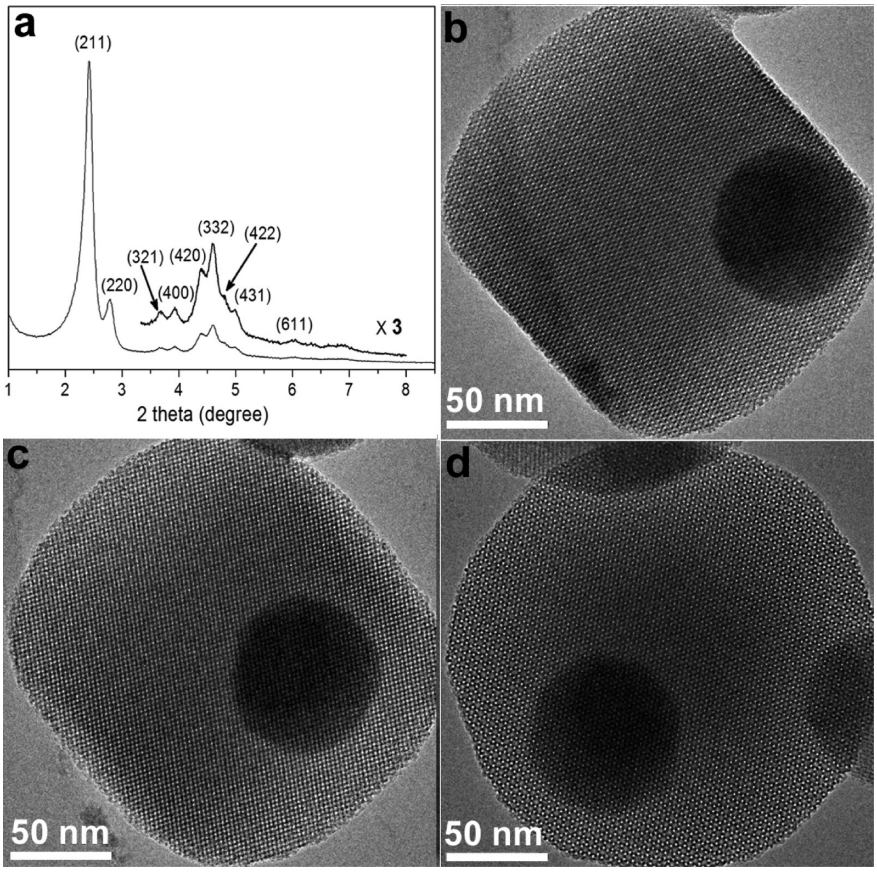

Figure 2. (a) Indexed powder XRD pattern of MCM-48 synthesized from S2-C14 surfactant. (b−d) HRTEM images of a MCM-48 particle recorded with different incidences ((b) [531], (c) [210], and (d) [111]).

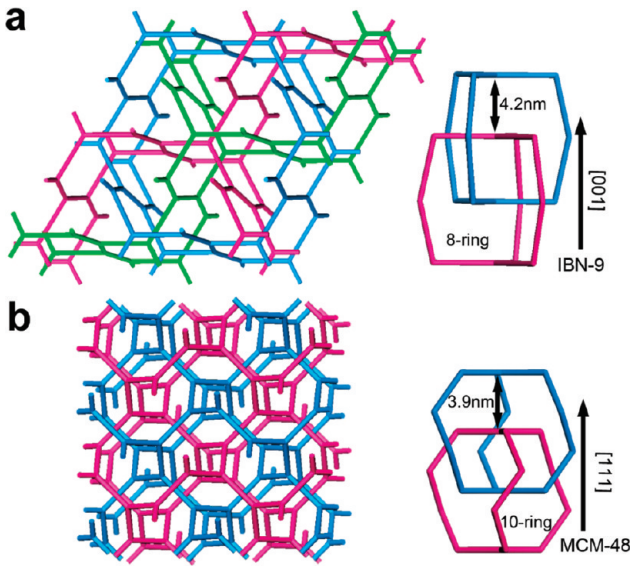

Figure 3. (a) The three interwoven channel systems of IBN-9 represented by three rod networks (2 × 2 × 2 unit cells) that follow the **etc-c3** net. (b) The two interwoven channel systems of MCM-48 represented by two rod networks (2 × 2 × 2 unit cells) that follow the **srs-c** net. On the right is part of the rod network isolated from each interpenetrating net. The similarity and difference between the channels in IBN-9 and MCM-48 are indicated.

of MCM-48 for comparison. Clearly, both structures are interpenetrating with three-connected channels, but the former consists of 8-membered rings while the latter consists of 10-membered rings. The distances between two 3-connected notes are 4.2 nm for IBN-9 (along the [001] direction) and 3.9 nm for MCM-48 (along the [111] direction) (see Figure 3). This distance corresponds to the sum of channel diameter and pore wall thickness. According to the channel diameters (2.7 nm for MCM-48 and 3.0 nm for IBN-9), it is concluded that IBN-9 and MCM-48 synthesized from the S2-C14 surfactant have the same silica wall thickness (1.2 nm).

Mesophase Transition and Synthesis Space Diagrams. A series of samples were synthesized from the typical synthesis conditions for IBN-9 by adjusting the concentration of ammonia solution from 2% to 30%. XRD patterns clearly showed the phase transition from tricontinuous IBN-9 to bicontinuous MCM-48 as the ammonia concentration increased (see Figure 4). IBN-9 was obtained when the ammonia concentration was ≤10%, while highly concentrated ammonia solution (≥20%) gave rise to the formation of the MCM-48 structure. For both IBN-9 and MCM-48, the XRD peaks shift to higher angles when synthesized with higher ammonia concentration, because the stronger alkalinity facilitated condensation of the silicate framework, resulting in unit-cell shrinkage. The particle morphology varies with the ammonia concentration as well. For example, IBN-9 synthesized from 5% ammonia solution consisted of short rods (2−5 μm

dx.doi.org/10.1021/cm2016593 |*Chem. Mater.* 2011, 23, 3775–3786

long) rather than long fibers as prepared from 2% ammonia solution (see Figure 4). When the ammonia concentration was increased to 10%, the dimension in the *c*-axis direction was further shortened and most IBN-9 particles became disklike. The sample prepared from a 15 wt % ammonia solution showed irregular particle morphology and only one XRD peak, suggesting a disordered structure. When a 25 wt % ammonia solution was used, MCM-48 phase was obtained in the form of submicrometer-sized cubic particles and such morphology was not changed with further increases in the ammonia concentration up to 30% (see Figure 4). Since "morphology" is related to the point-group symmetry of the crystal, it is not surprising to see fibers/rods for hexagonal IBN-9, irregular particles for the disordered material, and cubes for cubic MCM-48. However, it is worthy of note that long fibers can only be prepared with low ammonia concentration (<5 wt %) under static conditions.[28a,35] In addition, nonstructured silica gel would be obtained if the ammonia concentration is too low (<0.5 wt %).

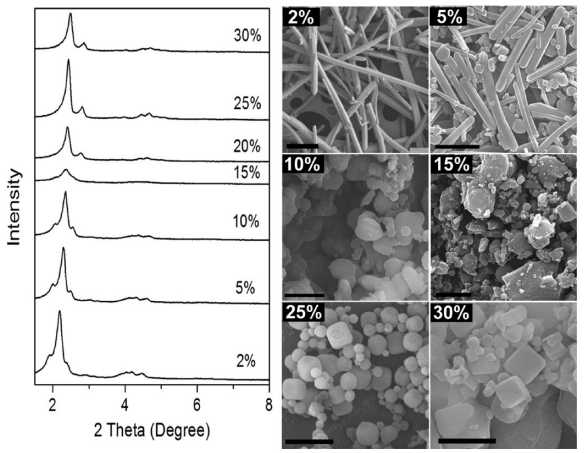

Figure 4. Powder XRD patterns (left) and SEM images (right) of a series of mesoporous silica materials synthesized from S2-C14 surfactant with increasing ammonia concentration from 2% to 30%. The scale bars correspond to 1 μm.

It has been indicated in our previous study that IBN-9 has a higher surface mean curvature than MCM-48 synthesized from the same surfactant template.[28] The phase transition from IBN-9 to MCM-48 by increasing the ammonia concentration can therefore be easily understood. The stronger alkalinity associated with a higher ammonia concentration would lead to a higher negative charge density of the silicate species. To maintain the charge density matching, the cationic surfactant molecules would adopt a more compact packing to form micelles with lower mean

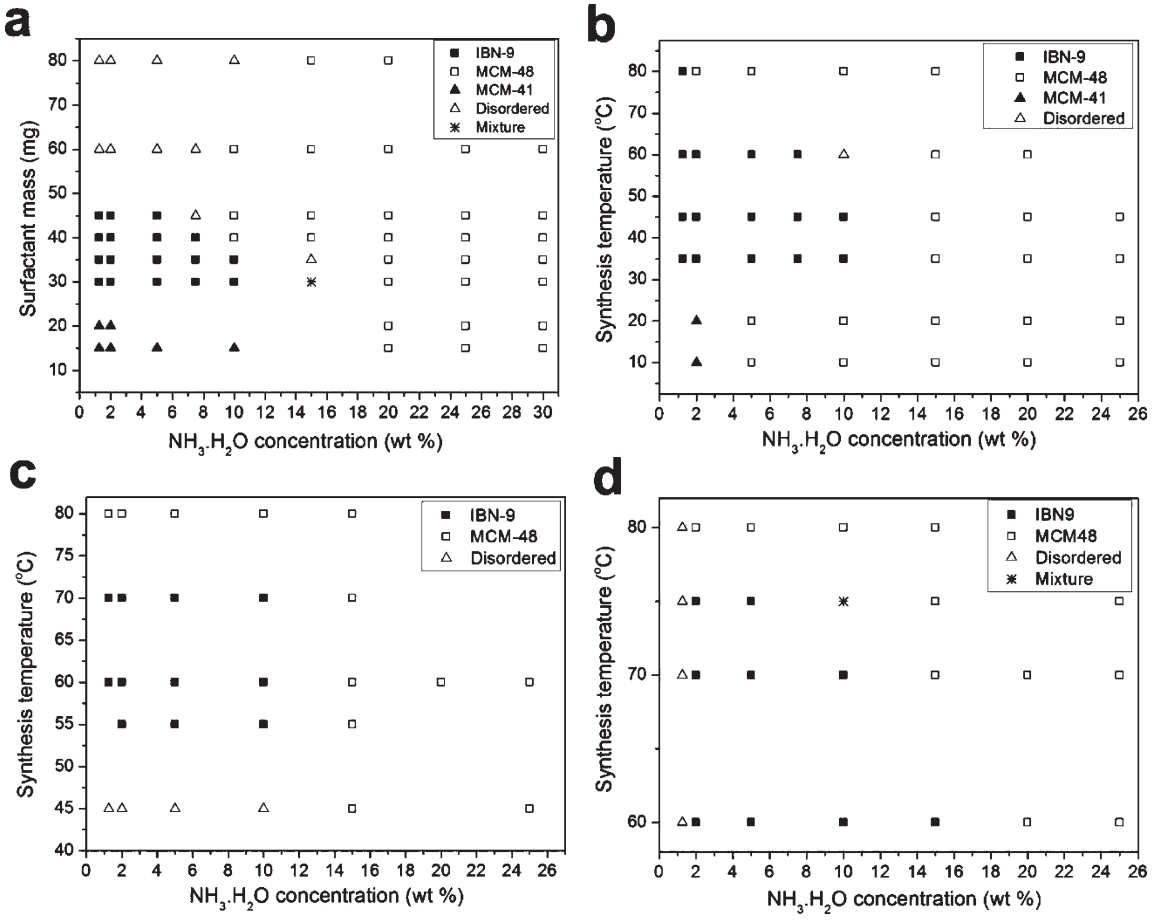

Figure 5. (a) Diagram of mesophases synthesized from surfactant S2-C14 with different surfactant concentrations at 45 °C. (b–d) Diagrams of mesophases synthesized from surfactants (b) S2-C14, (c) S2-C16, and (d) S2-C18, at different temperatures with a fixed surfactant concentration (70 mM). In all the diagrams, each sample was synthesized using 0.15 mL of TEOS and 12 mL aqueous ammonia solution. Phase identification was done by indexing the diffraction peaks in the XRD pattern. "Disordered" refers to mesophases that show only one diffraction peak; "Mixture" refers to a mixture of IBN-9 and MCM-48, as determined by TEM.

dx.doi.org/10.1021/cm2016593 |*Chem. Mater.* 2011, 23, 3775–3786

curvatures when they cooperatively assembled with the silicate species into mesostructures.[25,26]

Synthesis space diagrams clearly show that, besides the solution alkalinity (ammonia concentration), the surfactant concentration and the synthesis temperature also affect the mesostructures. Higher surfactant concentrations favor the formation of MCM-48 (Figure 5a), which is consistent with previous studies on the phase transition between MCM-41 and MCM-48.[25,26] In the optimal ammonia concentration range (<10%) for synthesizing IBN-9, reducing the surfactant/TEOS molar ratio to <0.05 resulted in the formation of a 2-D hexagonal MCM-41 phase, while disordered mesostructures were formed if the surfactant/TEOS molar ratio was >0.15 (see Figure 5a). The effect of synthesis temperature on the mesostructures is shown in Figure 5b, where the surfactant/TEOS molar ratio is fixed to 0.1 for all of the syntheses. It was found that IBN-9 could be synthesized in the temperature range of 30−80 °C from 1.25 wt % ammonia solution, while increasing the ammonia concentration would narrow the temperature range of successful synthesis. MCM-48 phase appears over a large area in the diagram covering both high-temperature and low-temperature regions. MCM-41 phase appears only where both temperature and ammonia concentration are low. The synthesis space diagrams illustrate that surfactant S2-C14 is a suitable template for fabricating both tricontinuous and bicontinuous mesostructures in wide experimental conditions, and they also confirm that tricontinuous IBN-9 is an intermediate phase between the cubic bicontinuous MCM-48 and the 2-D hexagonal MCM-41. This is in line with our previous conclusion that was mainly made by comparing the surface mean curvatures of the three different mesophases (MCM-41 > IBN-9 > MCM-48) calculated from their reconstructed electrostatic potential maps.[28a] The surface curvatures were indeed controlled by the synthesis conditions, and the general trend is that stronger alkalinity, higher surfactant concentration, and elevated temperature favors the formation of a mesophase with lower surface curvature.[25]

The molecular geometry of the surfactant is another crucial factor that would influence the mesostructure. Such an effect can usually be well-explained by the surfactant packing parameter $g = V/(a_0 l)$, where V is the volume of the hydrophobic chain, a_0 the effective area of the polar headgroup, and l the chain length. In general, a smaller g-value favors the formation of a mesophase with higher surface mean curvatures. With the above knowledge, the synthesis conditions of IBN-9 can be further extended rationally. As shown in the synthesis phase diagrams (Figures 5a and 5b), surfactant S2-C14 can generate the IBN-9 structure only at low ammonia concentration (low pH region). In order to extend the synthesis condition for IBN-9 to higher pH regions, a modified surfactant (S3-C14) was used for the synthesis (Scheme 1), which has a larger headgroup (a_0) than S2-C14 and thus tends to produce a mesostructure with higher surface curvature under the same synthesis conditions. In this sense, increasing the alkalinity of the synthesis media has an opposing effect on the surface curvature of mesostructure against using surfactant with a larger headgroup. As a result, tricontinuous IBN-9 was successfully synthesized from concentrated (up to 25%) ammonia solution by a S3-C14 template (Figure 6a). However, low ammonia concentration (<5%) led to MCM-41 structure (Figure 6b). Understanding the roles of temperature, pH value, and surfactant molecular geometry allows for more precise and facile synthesis of IBN-9. On the other hand, the attempts to synthesize IBN-9 in acidic solution were not successful.

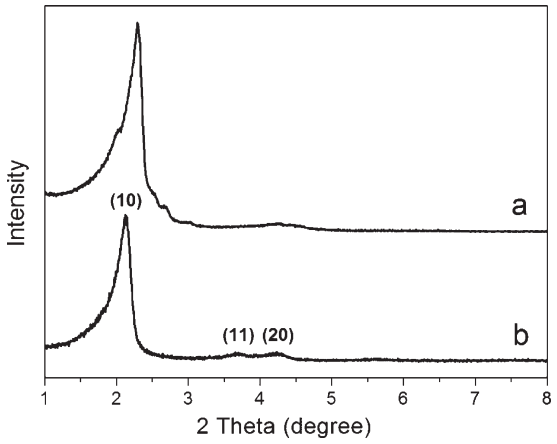

Figure 6. XRD patterns of mesoporous silica synthesized from (a) 25% ammonia solution and (b) 2.0% ammonia solution using surfactant S3-C14 as a template. The syntheses were carried out by following the typical procedure for IBN-9 synthesis, except that 42 mg of S3-C14 was used instead of 40 mg of S2-C14.

Pore Size Enlargement. Many applications of mesoporous materials rely on the precise control of their pore sizes;[36−38] therefore, for a newly developed mesostructure, it is highly desirable to achieve extensive adjustment of its pore size. To this end, two new surfactants—S2-C16 and S2-C18 (Scheme 1), with longer hydrocarbon chains than S2-C14—were used as a template. It was found that they showed similar structural-directing behaviors as S2-C14, giving rise to the IBN-9 structure in low concentration ammonia solution and the MCM-48 structure in high concentration ammonia solution, while elevated synthesis temperatures were needed, because of their poor solubility (see Figures 5c and 5d). The XRD results clearly illustrated that, with increasing the surfactant length, the unit cell of IBN-9 gradually became larger, as evidenced by the low-angle shifted peaks, while the c/a ratio was barely changed (Figure 7a). Accordingly, the capillary condensation step in the N_2 sorption isotherm shifted toward the high-pressure region (Figure 7b). The calculated pore sizes of IBN-9 synthesized from S2-C14, S2-C16, and S2-C18 are 3.0, 3.55, and 3.75 nm, respectively, indicating a successful enlargement of the tricontinuous channel diameter by 25% (Table 1). Moreover, the BET surface area and the pore volume of IBN-9 were also enhanced with the increase of pore size. Using S2-C18 to replace S2-C14, for example, achieved a 75% enhancement in the total pore volume, from 0.84 cm^3/g to 1.26 cm^3/g (Table 1). SEM revealed that the enlargement of pore size resulted in shorter IBN-9 fibers (Figure 8). Although the XRD patterns became poorly resolved as the pore size increased (Figure 7a), HRTEM confirmed that the samples synthesized from longer surfactants had the same tricontinuous structure (see Figures 8a and 9).

Helical mesoporous silica materials with twisted 1-D channels have been extensively studied.[8,39−42] The helical structure can be identified with TEM from two typical phenomena: (i) periodical and intermittent lattice fringes; and (ii) lattice fringes moving along the channel direction with tilting the TEM specimen. Interestingly, similar phenomena are frequently observed in IBN-9 samples synthesized with longer surfactants. This suggests a 3-D helical mesostructure with interwoven channels, which, to the best of our knowledge, has never been reported previously. Figure 9a is the TEM image of an IBN-9 fiber synthesized from

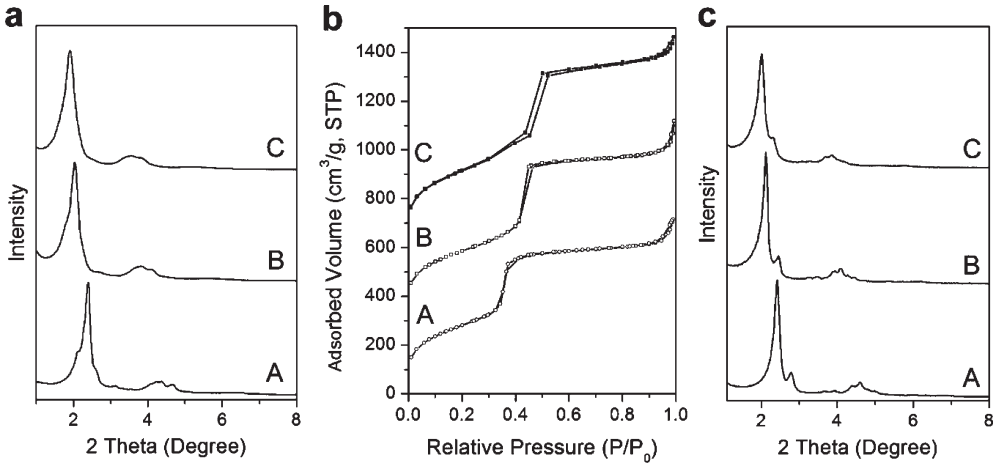

Figure 7. (a) XRD patterns and (b) N_2 sorption isotherms of IBN-9 synthesized using different surfactants (S2-C14 (spectrum A), S2-C16 (spectrum B), and S2-C18 (spectrum C)). (c) XRD patterns of MCM-48 synthesized from different surfactants (S2-C14 (spectrum A), S2-C16 (spectrum B), and S2-C18 (spectrum C)).

Table 1. Textural Properties of Mesoporous Silica IBN-9 and Mesoporous Carbon IBN-9-C[a]

	BET surface area (m^2/g)	pore diameter (nm)	pore volume (cm^3/g)[b]
IBN-9 (S2-C14)	842	3.0	0.84
IBN-9 (S2-C16)	1128	3.55	1.09
IBN-9 (S2-C18)	1073	3.75	1.26
IBN-9-C[c]	1788 (1960)	0.7/1.65/3.36	1.56

[a] The data are based on nitrogen sorption experiments, except those of IBN-9-C that are obtained from the argon adsorption results. The pore diameters of IBN-9 silicas are determined by Barrett—Joyner—Halenda (BJH) method, whereas NLDFT method is used for IBN-9-C. [b] Single-point total pore volume at $P/P_0 = 0.95$. [c] IBN-9-C is synthesized using IBN-9 (S2-C14) as a template. The BET surface area given in the parentheses is determined from the nitrogen sorption isotherm.

S2-C18, showing two small regions with ordered patterns (marked with squares), which are separated by ~550 nm and correspond to the lattice fringes of [100] and [1$\bar{1}$0] incidences, respectively. Figure 9b shows another fiber with similar intermittent [100] and [1$\bar{1}$0] lattice fringes that are also separated by ~550 nm along the fiber axis. Notably, the appearance of intermittent lattice fringes does not mean that the ordered structure is discontinuous. As indicated by the arrows in Figures 9c and 9d, the lattice patterns smoothly moved along the fiber when the TEM specimen was tilted along an axis parallel to the fiber. This means that, with sample tilting, the [100] zone axis at different positions along the fiber were sequentially turned to be parallel to the beam, showing the structure projection. This phenomenon clearly demonstrates the helical nature of the mesostructure, which can be considered as a twisted form of the original tricontinuous IBN-9 structure (see Figures 9e and 9f). Given that the angle between [100] and [1$\bar{1}$0] incidences is 30°, the structure is twisted by 30° between the two sets of lattice fringes. Therefore, the helical pitch is 12 times the distance between the adjacent [100] and [1$\bar{1}$0] fringes (i.e., ~6.6 μm). Compared to the pitch length, the particles are too short (~1 μm) to show helical (twisted) morphologies in the SEM image (Figure 8b). The driving force for helical tricontinuous structure formation is not well-understood, yet it is apparently associated

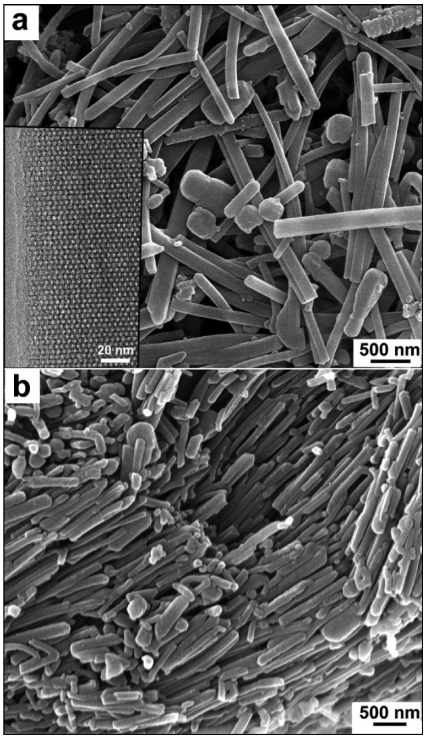

Figure 8. (a) SEM image of IBN-9 synthesized from surfactant S2-C16 in 2% ammonia solution at 60 °C. Insert is a HRTEM image taken along the [1$\bar{1}$0] direction. (b) SEM image of IBN-9 synthesized using surfactant S2-C18 in 2% ammonia solution at 70 °C.

with the use of the longer-chain surfactants, since such structure is less common in IBN-9 prepared from S2-C16, compared to that from S2-C18, and is rarely observed when S2-C14 is used as a template. The twisting of the mesostructure that increased the anisotropic microstrains may account for the broadened and less-well-resolved XRD peaks of IBN-9 synthesized with long surfactants.

In a high-concentration ammonia solution, S2-C16 and S2-C18 could template MCM-48 structures with enlarged unit cells (see Figure 7c) and pore sizes (3.45 nm for S2-C16 and 3.63 nm

dx.doi.org/10.1021/cm2016593 |Chem. Mater. 2011, 23, 3775–3786

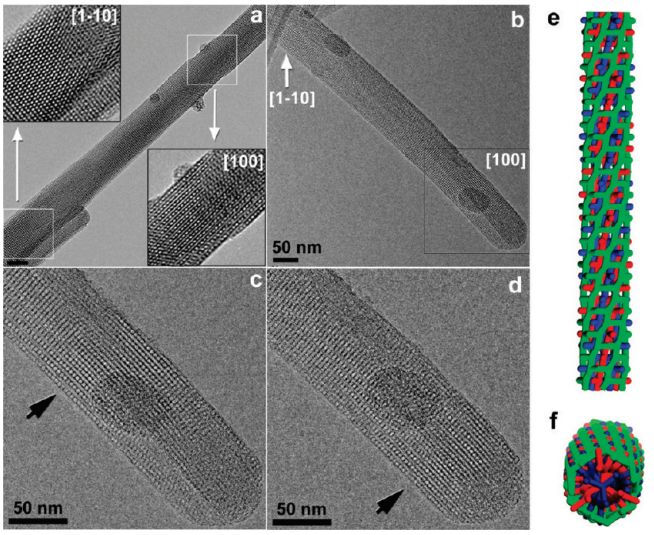

Figure 9. (a) HRTEM image of an IBN-9 fiber synthesized using surfactant S2-C18, showing both [100] and [1$\bar{1}$0] lattice fringes at different positions that are enlarged in the insets. The scale bar corresponds to 50 nm. (b) TEM image of another IBN-9 fiber with discontinuous lattice fringes. (c) HRTEM image of the marked area in panel (b). (d) HRTEM image of the same area as in panel (c) after tilting the fiber by 5°. The black arrows in panels (c) and (d) indicate the movement of the [100] fringes with the tilting. A proposed structural model of the helical IBN-9 with the three interwoven 3D channel systems represented by rod networks in different colors viewed (e) perpendicular to the fiber axis and (f) along the fiber axis.

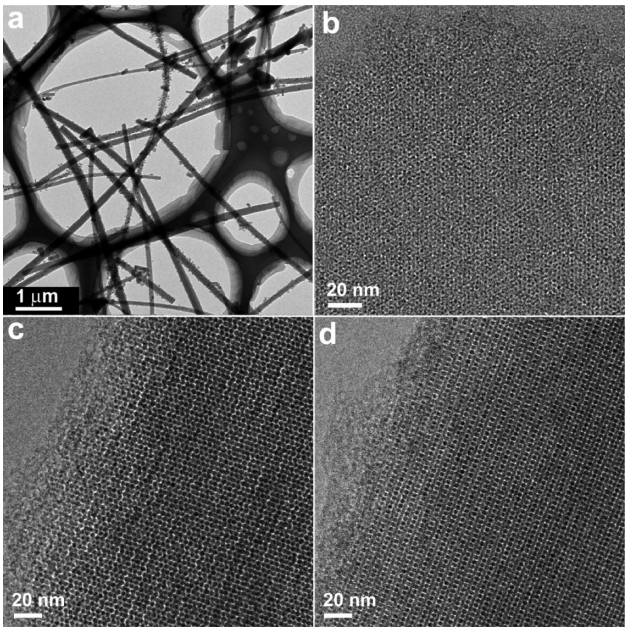

Figure 10. (a) Low-magnification TEM image of IBN-9-C, showing the nanofiber morphology replicated from the IBN-9 silica material. (b–d) HRTEM images of IBN-9-C taken along the (b) [001], (c) [1$\bar{1}$0], and (d) [100] directions. Ultramicrotome was applied to cut the carbon fibers into thin slices, to acquire the image along the [001] direction.

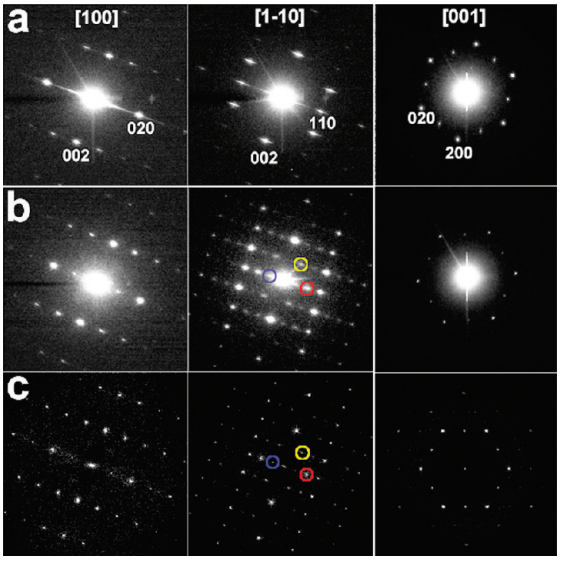

Figure 11. (a) SAED patterns of IBN-9 recorded along the [100], [1$\bar{1}$0], and [001] directions. The corresponding HRTEM images are shown in Figures 1c, 1d, and 1e, respectively. (b) SAED patterns and (c) Fourier diffractograms from HRTEM images of IBN-9-C taken along the [100], [1$\bar{1}$0], and [001] directions. The corresponding HRTEM images are shown in Figure 10d, 10c, and 10b, respectively. In panels (b) and (c), the reflections marked in red, yellow, and blue have indices of ($^2/_3$ $^2/_3$ 0), ($^1/_3$ $^1/_3$ 1), and ($-^1/_3$ $-^1/_3$ 0), respectively; all other reflections have the same indices as their counterparts in panel (a).

for S2-C18), in the same way as they did for IBN-9 in low-concentration ammonia solution. Further enlargement in pore sizes cannot be achieved for IBN-9 or MCM-48 by simply further extending the length of this type of surfactant, because it would make the surfactant insoluble. Also, 1,3,5-trimethylbenzene (TMB) was used as a swelling agent for IBN-9 synthesis with S2 series surfactants. However, the tricontinuous structure was destroyed upon the addition of TMB. Bicontinuous $Ia\bar{3}d$ structures with a pore size of >6 nm have been successfully prepared by using block copolymer as a template.[15,16] We expect that the tricontinuous $P6_3/mcm$ mesostructure could also be fabricated with other types of surfactant and this will allow for further pore size adjustment.

"Hard-Templating" Synthesis with IBN-9. Hard-templating (nanocasting) strategy has been widely used for synthesizing various mesostructured materials from mesoporous silicas.[43−59] Tricontinuous IBN-9 has a very open 3-D porous system that makes it an ideal "hard template". In this study, a new mesoporous carbon material (IBN-9-C) was fabricated using furfuryl alcohol as a carbon precursor and IBN-9 as a "hard template". TEM images indicate that IBN-9-C well replicate both the fiber morphology (Figure 10a) and the highly ordered mesostructure (Figures 10b–d). While the SAED patterns are similar for IBN-9-C and IBN-9 (see Figures 11a and 11b), the corresponding HRTEM images show inverted contrast (see Figures 1 and 10, and Figure S2 in the Supporting Information), suggesting that IBN-9-C is basically a negative replica of the silica IBN-9. However, it is noticed that the [1$\bar{1}$0] SAED pattern of IBN-9-C exhibits a few more reflections with large d-values, compared to its counterpart for IBN-9. Accordingly, two additional peaks appear in the XRD pattern at 2θ = 1.40° and 1.88° (Figure 12a). The extra reflections in the SAED and XRD patterns indicate that IBN-9-C has a superstructure, compared to the silica IBN-9. These reflections can be indexed using fractional indices, i.e., ($^1/_3$ $^1/_3$ 0), ($^2/_3$ $^2/_3$ 0), and ($^1/_3$ $^1/_3$ 1) (Figures 11b and 12a),

dx.doi.org/10.1021/cm2016593 |Chem. Mater. 2011, 23, 3775–3786

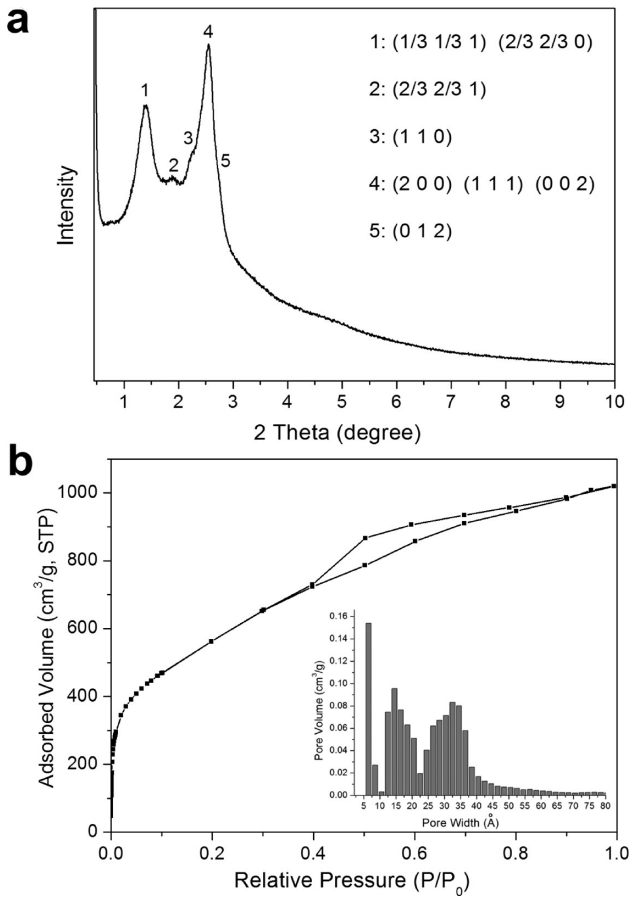

Figure 12. (a) Indexed XRD pattern and (b) argon adsorption/desorption isotherm of IBN-9-C. Inset shows the NLDFT volume histogram based on the isotherm, showing three major pore size distributions centered at 7.0, 16.5, and 33.6 Å, respectively.

which suggests a hexagonal superlattice for IBN-9-C with $a_{\text{IBN-9-C}} = 3^{1/2}a_{\text{IBN-9}}$. The HRTEM image along the $[1\bar{1}0]$ direction shows a set of regularly spaced bright fringes that corresponds to the $(^1/_3\ ^1/_3\ 0)$ reflection (see Figure 10c and Figure S3 in the Supporting Information). The corresponding Fourier transform is consistent with the SAED pattern, showing superstructure reflections (Figure 11c). If one ignores these superstructure reflections and uses the remaining for structure reconstruction, it is found that the main reflections have exactly reversed structure factor phases in comparison with those of IBN-9 (Table 2). As a result, a perfect "negative replica" of IBN-9 is reconstructed that consists of three 3-D interpenetrating carbon networks (Figure 13). However, the appearance of additional reflections in SAED and XRD suggests that IBN-9-C is not simply a negative replica of the tricontinuous structure but rather a "superlattice" possibly generated by some structural defects. This phenomenon may be caused by two possible reasons, i.e., incomplete filling of the mesoporous channel by carbon and displacement of the carbon networks during the dissolution of silica template. In previous studies on CMK-1, which is the carbon replica of MCM-48, similar phenomenon (i.e., the appearance of new diffraction peaks) was attributed to the lowered symmetry caused by the displacement of the carbon networks. However, different models for the "displacement" were proposed without a definitive solution.[45,46] The case of

Table 2. Crystal Structure Factors of IBN-9 and IBN-9-C[a]

	IBN-9		IBN-9-C	
hkl	amplitude	phase	amplitude	phase
1 1 0	3500	0	5398	180
0 0 2	6293	0	9269	180
1 1 1	4616	0	6039	180
0 2 0	10000	180	10000	0
0 1 2	3618	0	4268	180
1 2 0	1003	0	711	180
0 3 0	581	0	633	180
2 2 0	1080	0	799	180
1 3 0	842	180	832	0
0 0 4	678	0	830	180
0 4 0	775	0	926	180

[a] The amplitudes and phases of the structure factor $F(hkl)$ were obtained from the HRTEM images using the program CRISP.[34] The amplitudes were normalized to the strongest reflection (020).

IBN-9-C is even more complicated, because it contains one more dimension of carbon network dispersion, compared to CMK-1. We notice that the superstructure reflections are only visible in the SAED pattern and HRTEM image along the $[1\bar{1}0]$ direction, but do not appear in the SAED patterns and HRTEM images along the [100] and [001] directions. We are currently trying to build a structural model explaining these superstructure reflections, but this is still a great challenge, because of the structure complexity.

IBN-9-C possesses apparently higher specific surface area, in comparison with other ordered mesoporous carbon materials synthesized via "hard-templating" routes.[43−50] It is generally believed that nitrogen BET method overestimates the surface area of carbons with relatively narrow pores, while the result of argon BET analysis is more accurate.[44,59] The BET surface area of IBN-9-C is 1960 m^2/g and 1788 m^2/g, as determined from nitrogen adsorption isotherm and argon adsorption isotherm, respectively (see Figure 12b and Table 1). In contrast, most of the other templated mesoporous carbon materials have argon BET surface areas of <1400 m^2/g.[43−49] Moreover, IBN-9-C has a total pore volume as high as 1.56 cm^3/g, as determined from the argon sorption isotherm at $P/P_0 = 0.95$ (Table 1). The pore system of IBN-9-C is complex, having three major pore width distributions centered at 7.0, 16.5, and 33.6 Å, respectively, as calculated using a nonlocal density functional theory (NLDFT) slit pore model (Figure 12b, inset). This complexity is supposed to be associated with the displacement or incomplete filling of the carbon networks and explains the relative flatness of the capillary condensation steps on the adsorption isotherms (Figure 12b). Notably, micropores (<1 nm) in the adsorbent are desired for gas adsorption which can provide additional potential for trapping the gas molecules at low pressure. The combination of large specific surface area, high pore volume, and a significant amount of micropores endows IBN-9-C with remarkable gas adsorption capability at both cryogenic temperatures and room temperature. For example, the H_2 uptake at 1 bar in IBN-9-C is 2.02 wt % at 77 K and 1.49 wt % at 87 K. The initial value of isosteric heat of adsorption (Q_{st}) for hydrogen in IBN-9-C is calculated to be 8.98 kJ/mol. Also, IBN-9-C exhibits a significant uptake of CO_2 at 1 bar (5.26 mmol/g at 258 K, 2.60 mmol/g at 298 K, and 1.56 mmol/g at 328 K), and the corresponding initial Q_{st} is 31.0 kJ/mol.

dx.doi.org/10.1021/cm2016593 |*Chem. Mater.* 2011, 23, 3775–3786

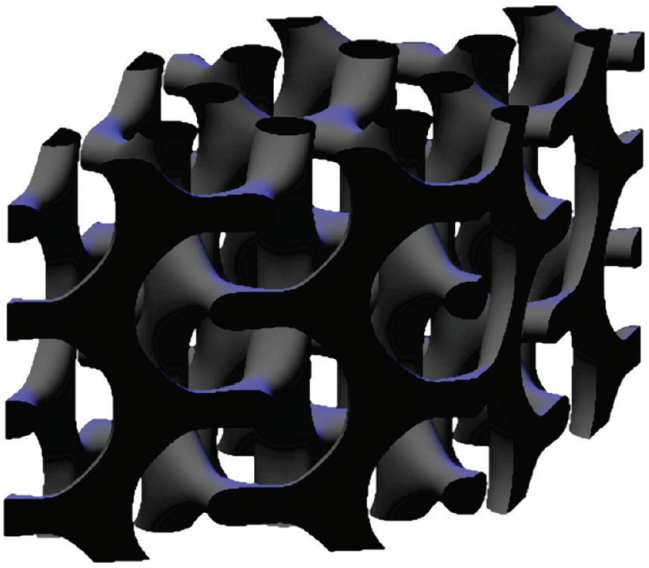

Figure 13. The reconstructed 3D carbon framework of IBN-9-C using the crystal structure factors extracted from the three HRTEM images shown in Figures 10b−d. The structure factors are listed in Table 2. The superstructure reflections (see Figure 11) were ignored in the structure reconstruction. The threshold that defines the carbon surface was determined by the pore volume from the N_2 adsorption.

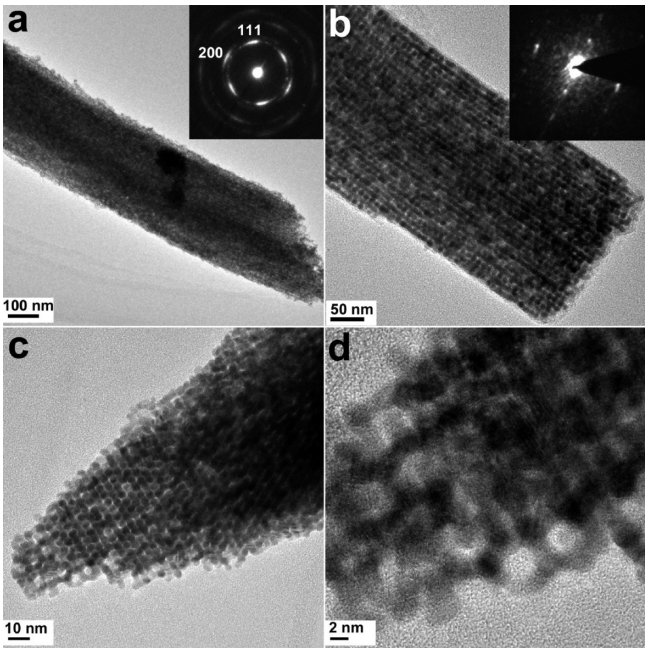

Figure 14. TEM images of several individual IBN-9-Pt nanofibers. (a) Low-magnification image (inset is the corresponding SAED pattern taken at a short camera length of 40 cm; the arclike diffraction spots indicate that the Pt nanocrystals are highly oriented). (b) High-magnification image and the corresponding SAED pattern (inset) taken at a long camera length of 3 m; the diffraction spots show the structural ordering at mesoscopic scale. (c,d) HRTEM images showing incomplete replication at the edge of a fiber, where platinum replicated only one of the three channels of IBN-9.

These gas uptake and Q_{st} values are rather high, considering that IBN-9-C is a pure carbon material without any surface modification or doping, and can be attributed to its special textual properties. More-detailed investigation of gas adsorption/storage in IBN-9-C will be reported separately.

Widespread potential applications in areas ranging from catalysis and optics to biotechnology have been demonstrated for noble-metal nanoarrays.[60,61] It would also be interesting to synthesize a 3-D mesostructured metal framework with coincident crystal orientation, although it has been observed that indium oxide[55] and tungsten sulfide[56] crystals formed in SBA-15 template are partially oriented by the 1-D channels. In a proof-of-concept experiment, we synthesized platinum in the channels of the IBN-9 "hard template". After completely removing the silica, the obtained platinum material (IBN-9-Pt) exhibits fiber morphology analogous to the template, but the length is much shorter, because of the severe volume shrinkage during the reduction of the precursor to platinum metal (see Figure S4 in the Supporting Information). Figure 14 shows the TEM images of several individual mesostructured platinum fibers taken at different magnifications. The platinum material has structural ordering in two different length scales: mesoscopic and atomic. When a large camera length (3 m) is used, diffraction spots with *d*-values of 3.4 and 2.1 nm can be clearly observed in the SAED pattern, corresponding to the (020) and (004) reflections of the ordered mesostructure that is replicated from IBN-9 (see Figure 14b and inset). On the other hand, the SAED taken with a short camera length (40 cm) shows short diffraction arcs rather than polycrystalline diffraction rings. The flare angle of each diffraction arc is ∼25° (Figure 14a, inset). This result illustrates that the 3-D network is composed of platinum nanocrystals with highly coincident [100] orientation that is parallel to the long axis of the fiber. Such preferential orientation should be related to the confined crystal growth within the anisotropic nanochannels of IBN-9. To our knowledge, this is the first time that a 3-D mesostructured metal network with highly oriented crystals has been fabricated. Most of the platinum fibers completely replicate the tricontinuous mesoporous structure, forming densely interpenetrating networks (see Figures 14a and 14b). However, incomplete replication, with only one or two of the three channels replicated, occurs at the edges/ends of certain fibers, where an open platinum framework with large pores can be observed (see Figures 14c and 14d). Incomplete replication is actually a common phenomenon when "bi-continuous" mesoporous silica materials are used as a hard template.[51,55,56]

■ CONCLUSIONS

Precisely controlled synthesis of the first tricontinuous mesoporous material IBN-9 has been achieved using a series of specially designed surfactants as a template. The same surfactants can also template the synthesis of bicontinuous cubic MCM-48 and two-dimensional (2-D) hexagonal MCM-41 under different synthetic conditions. The synthesis space diagrams have been carefully investigated for the three related mesophases, and the results confirm that IBN-9 is an intermediate phase between MCM-48 and MCM-41. Rational modification of the surfactant template allows for the extension of synthesis conditions for IBN-9 and enlarges its channel diameter by ∼25%. An unprecedented three-dimensional (3-D) helical mesoporous structure formed by twisting the 3-fold interpenetrating channels system is also synthesized. IBN-9 has proven to be a good hard template for the nanocasting synthesis of mesostructured materials with other functional compositions, e.g. carbon and platinum, which successfully replicated not only the tricontinuous structure but

also the unique nanofiber morphology of IBN-9. The obtained mesoporous carbon material exhibits large surface area, as well as high pore volume, and, thus, remarkable gas adsorption capability.

■ ASSOCIATED CONTENT

Supporting Information. HRTEM images and SAED pattern of IBN-9, IBN-9-C, and IBN-9-Pt; experimental details of the synthesis of surfactant S3-C14; and detailed procedures for resolving the structure of IBN-9. This information is available free of charge via the Internet at http://pubs.acs.org.

■ AUTHOR INFORMATION

Corresponding Author
*E-mail: yu.han@kaust.edu.sa.

■ ACKNOWLEDGMENT

This work was supported by the Collaboration Travel Fund from King Abdullah University of Science and Technology, the Swedish Research Council (VR), the Swedish Governmental Agency for Innovation Systems (VINNOVA), and the Göran Gustafsson Foundation. Y.H. thanks Dr. Leng Leng Chng for developing the synthetic routes for the surfactants.

■ REFERENCES

(1) Beck, J. S.; Vartuli, J. C.; Roth, W. J.; Leonowicz, M. E.; Kresge, C. T.; Schmitt, K. D.; Chu, C. T. W.; Olson, D. H.; Sheppard, E. W. *J. Am. Chem. Soc.* **1992**, *114*, 10834.
(2) Inagaki, S.; Fukushima, Y.; Kuroda, K. J. *Chem. Soc. Chem. Commun.* **1993**, 680.
(3) Monnier, A.; Schuth, F.; Huo, Q.; Kumar, D.; Margolese, D.; Maxwell, R. S.; Stucky, G. D.; Krishnamurty, M.; Petroff, P.; Firouzi, A.; Janicke, M.; Chmelka, B. F. *Science* **1993**, *261*, 1299.
(4) Huo, Q. S.; Margolese, D. I.; Ciesla, U.; Feng, P. Y.; Gier, T. E.; Sieger, P.; Leon, R.; Petroff, P. M.; Schüth, F.; Stucky, G. D. *Nature* **1994**, *368*, 317.
(5) Attard, G. S.; Glyde, J. C.; Goltner, C. G. *Nature* **1995**, *378*, 366.
(6) Yang, P. D.; Zhao, D. Y.; Margolese, D. I.; Chmelka, B. F.; Stucky, G. D. *Nature* **1998**, *396*, 152.
(7) Zhao, D. Y.; Huo, Q. S.; Feng, J. L.; Chmelka, B. F.; Stucky, G. D. *J. Am. Chem. Soc.* **1998**, *120*, 6024.
(8) Che, S.; Liu, Z.; Ohsuna, T.; Sakamoto, K.; Terasaki, O.; Tatsumi, T. *Nature* **2004**, *429*, 281.
(9) Kleitz, F.; Liu, D. N.; Anilkumar, G. M.; Park, I. S.; Solovyov, L. A.; Shmakov, A. N.; Ryoo, R. *J. Phys. Chem. B* **2003**, *107*, 14296.
(10) Yu, C. Z.; Tian, B. Z.; Fan, J.; Stucky, G. D.; Zhao, D. Y. *J. Am. Chem. Soc.* **2002**, *124*, 4556.
(11) Sakamoto, Y.; Kaneda, M.; Terasaki, O.; Zhao, D. Y.; Kim, J. M.; Stucky, G. D.; Shin, H. J.; Ryoo, R. *Nature* **2000**, *408*, 449.
(12) Garcia-Bennett, A. E.; Miyasaka, K.; Terasaki, O. *Chem. Mater.* **2004**, *16*, 3597.
(13) Carlsson, A.; Kaneda, M.; Sakamoto, Y.; Terasaki, O.; Ryoo, R.; Joo., S. H. *J. Electron Microsc.* **1999**, *48*, 795.
(14) Shin, H. J.; Ryoo, R.; Liu, Z.; Terasaki, O. *J. Am. Chem. Soc.* **2001**, *123*, 1246.
(15) Kleitz, F.; Choi, S. H.; Ryoo, R. *Chem. Commun.* **2003**, 2136.
(16) Liu, X. Y.; Tian, B. Z.; Yu, C. Z.; Gao, F.; Xie, S. H.; Tu, B.; Che, R. C.; Peng, L. M.; Zhao, D. Y. *Angew. Chem.; Int. Ed.* **2002**, *41*, 3876.
(17) Gao, C.; Sakamoto, Y.; Sakamoto, K.; Terasaki, O.; Che, S. *Angew. Chem., Int. Ed.* **2006**, *45*, 4295.
(18) Finnefrock, A. C.; Ulrich, R.; Du Chesne, A.; Honeker, C. C.; Schumacher, K.; Unger, K. K.; Gruner, S. M.; Wiesner, U. *Angew. Chem., Int. Ed.* **2001**, *40*, 1208.
(19) Enlow, J. D.; Enlow, R. L.; McGrath, K. M.; Tate, M. W. *J. Chem. Phys.* **2004**, *120*, 1981.
(20) Barois, P.; Hyde, S.; Ninham, B.; Dowling, T. *Langmuir* **1990**, *6*, 1136.
(21) Radiman, S.; Toprakcioglu, C.; Dai, L.; Faruqi, A. R. *Colloq. Phys.* **1990**, *C7*, 51.
(22) Maddaford, P. J.; Toprakcioglu, C. *Langmuir* **1993**, *9*, 2868.
(23) Linhananta, A.; Sullivan, D. E. *Phys. Rev. E* **1998**, *57*, 4547.
(24) Hyde, S. T. Identification of lyotropic liquid crystalline mesophases. In *Handbook of Applied Surface and Colloid Chemistry*; Holmberg, K. Ed.; Wiley: New York, 2001; Chapter 16, p 299.
(25) Huo, Q. S.; Margolese, D. I.; Stucky, G. D. *Chem. Mater.* **1996**, *8*, 1147.
(26) Wan, Y.; Zhao, D. Y. *Chem. Rev.* **2007**, *07*, 2821.
(27) Che, S.; Garcia-Bennett, A. E.; Yokoi, T.; Sakamoto, K.; Kunieda, H.; Terasaki, O.; Tatsumi, T. *Nat. Mater.* **2003**, *2*, 801.
(28) (a) Han, Y.; Zhang, D. L.; Chng, L. L.; Sun, J. L.; Zhao, L.; Zou, X. D.; Ying, J. Y. *Nature Chem.* **2009**, *1*, 121. (b) Zhang, D. L.; Sun, J. L.; Han, Y.; Zou, X. D. *Microporous Mesoporous Mater.* **2011**, in press (DOI: 10.1016/j.micromeso.2011.05.026).
(29) Ryoo, R. *Nature Chem.* **2009**, *1*, 105.
(30) Hyde, S. T. *Curr. Opin. Solid State Mater.* **1996**, *1*, 653.
(31) Hyde, S. T.; Schröder, G. E. *Curr. Opin. Colloid Interface Sci.* **2003**, *8*, 5.
(32) Hyde, S. T.; de Campo, L.; Oguey, C. *Soft Matter* **2009**, *5*, 2782.
(33) Brakke, K. *Exp. Math.* **1992**, *1*, 141.
(34) Hovmöller, S. *Ultramicroscopy* **1992**, *41*, 121.
(35) Huo, Q.; Zhao, D.; Feng, J.; Weston, K.; Buratto, S. K.; Stucky, G. D.; Schacht, S.; Schüth., F. *Adv. Mater.* **1997**, *9*, 974.
(36) Ren, Y.; Robert Armstrong, A.; Jiao, F.; Bruce, P. G. *J. Am. Chem. Soc.* **2010**, *132*, 996.
(37) Han, Y.; Lee, S. S.; Ying, J. Y. *Chem. Mater.* **2007**, *19*, 2292.
(38) Zhao, Y.-L.; Li, Z.; Kabehie, S.; Botros, Y. Y.; Stoddart, J. F.; Zink, J. I. *J. Am. Chem. Soc.* **2010**, *132*, 13016.
(39) Ohsuna, T.; Liu, Z.; Che, S.; Terasaki, O. *Small* **2005**, *1*, 233.
(40) Han, Y.; Zhao, L.; Ying, J. Y. *Adv. Mater.* **2007**, *19*, 2454.
(41) Yang, S.; Zhao, L.; Yu, C.; Zhou, X.; Tang, J.; Yuan, P.; Chen, D.; Zhao, D. *J. Am. Chem. Soc.* **2006**, *128*, 10460.
(42) Wang, B.; Chi, C.; Shan, W.; Zhang, Y.; Ren, N.; Yang, W.; Tang, Y. *Angew. Chem., Int. Ed.* **2006**, *45*, 2008.
(43) Ryoo, R.; Joo, S. H.; Jun, S. *J. Phys. Chem. B* **1999**, *103*, 7743.
(44) Ryoo, R.; Joo, S. H. *J. Phys. Chem. B* **2000**, *104*, 7960.
(45) Kaneda, M.; Tsubakiyama, T.; Carlsson, A.; Sakamoto, Y.; Ohsuna, T.; Terasaki, O. *J. Phys. Chem. B* **2002**, *106*, 1256.
(46) Solovyov, L. A.; Zaikovskii, V. I.; Shmakov, A. N.; Belousov, O. V.; Ryoo, R. *J. Phys. Chem. B* **2002**, *106*, 12198.
(47) Lee, J.; Yoon, S.; Hyeon, T.; Oh, S. M.; Kim, K. B. *Chem Commun.* **1999**, 2177.
(48) Lee, J.; Yoon, S.; Oh, S. M.; Shin, C.-H.; Hyeon, T. *Adv. Mater.* **2000**, *12*, 359.
(49) Ueda, K.; Sato, Y.; Mori, M. *J. Am. Chem. Soc.* **2000**, *122*, 10712.
(50) Joo, S. H.; Choi, S. J.; Oh, I.; Kwak, J.; Liu, Z.; Terasaki, O.; Ryoo, R. *Nature* **2001**, *412*, 169.
(51) Shin, H. J.; Ryoo, R.; Liu, Z.; Terasaki, O. *J. Am. Chem. Soc.* **2001**, *123*, 1246.
(52) Huang, M. H.; Choudrey, A.; Yang, P. *Chem. Commun.* **2000**, 1063.
(53) Schüth, F. *Chem. Mater.* **2001**, *13*, 3184.
(54) Tian, B.; Liu, X.; Yang, H.; Xie, S.; Yu, C.; Tu, B.; Zhao, D. Y. *Adv. Mater.* **2003**, *15*, 1370.
(55) Yang, H.; Shi, Q.; Tian, B.; Lu, Q.; Gao, F.; Xie, S.; Fan, J.; Yu, C.; Tu, B.; Zhao, D. Y. *J. Am. Chem. Soc.* **2003**, *125*, 4724.
(56) Shi, Y.; Wan., Y.; Liu, R.; Tu, B.; Zhao, D. Y. *J. Am. Chem. Soc.* **2007**, *129*, 9522.
(57) Yang, H.; Shi, Q.; Tian, B.; Lu, Q.; Gao, F.; Xie, S.; Fan, J.; Yu, C.; Tu, B.; Zhao, D. Y. *J. Am. Chem. Soc.* **2003**, *125*, 4724.

(58) Shi, Y.; Guo, B.; Corr, S. A.; Shi, Q.; Hu, Y.-S.; Heier, K. R.; Chen, L.; Seshadri, R.; Stucky, G. D. *Nano Lett.* **2009**, *9*, 4215.
(59) Kruk, M.; Jaroniec, M.; Gadkaree, K. P. *Langmuir* **1999**, *15*, 1442.
(60) Daniel, M. C.; Astruc, D. *Chem. Rev.* **2004**, *104*, 293.
(61) Schmid, G.; Corain, B. *Eur. J. Inorg. Chem.* **2003**, 3081.

■ NOTE ADDED AFTER ASAP PUBLICATION

This article was published ASAP on June 20, 2011, with an incorrect citation for reference 28b. The corrected version was published ASAP on June 22, 2011.